Feature Article

Conduction Model of Metal Oxide Gas Sensors

NICOLAE BARSAN & UDO WEIMAR

Institute of Physical and Theoretical Chemistry, University of Tuebingen, Auf der Morgenstelle 8, 72076 Tübingen, Germany

Abstract. Tin dioxide is a widely used sensitive material for gas sensors. Many research and development groups in academia and industry are contributing to the increase of (basic) knowledge/(applied) know-how. However, from a systematic point of view the knowledge gaining process seems not to be coherent. One reason is the lack of a general applicable model which combines the basic principles with measurable sensor parameters.

The approach in the presented work is to provide a frame model that deals with all contributions involved in conduction within a real world sensor. For doing so, one starts with identifying the different building blocks of a sensor. Afterwards their main inputs are analyzed in combination with the gas reaction involved in sensing. At the end, the contributions are summarized together with their interactions.

The work presented here is one step towards a general applicable model for real world gas sensors.

Keywords: metal oxide, gas sensors, conduction model

1. Introduction

Metal oxides in general and SnO_2, in particular, have attracted the attention of many users and scientists interested in gas sensing under atmospheric conditions. SnO_2 sensors are the best-understood prototype of oxide-based gas sensors. Nevertheless, highly specific and sensitive SnO_2 sensors are not yet available. It is well known that sensor selectivity can be fine-tuned over a wide range by varying the SnO_2 crystal structure and morphology, dopants, contact geometries, operation temperature or mode of operation, etc. In addition, practical sensor systems may contain a combination of a filter (like charcoal) in front of the SnO_2 semiconductor sensor to avoid major impact from unwanted gases (e.g. low concentrations of organic volatiles which influence CO detection). The understanding of real sensor signals as they are measured in practical application is hence quite difficult. It may even be necessary to separate filter and sensor influences for an unequivocal modelling of sensor responses.

In spite of extensive world wide activities in the research and development of these sensors, our basic scientific understanding of practically useful gas sensors is very poor. This results from the fact that three different approaches are generally chosen by three different kinds of experts. Our present understanding is hence based on different models

- The first approach is chosen by the *users* of gas sensors, who test the phenomenological parameters of available sensors in view of a minimum parameter set to describe their selectivity, sensitivity, and stability.

- The second approach is chosen by the *developers*, who empirically optimise sensor technologies by optimising the preparation of sensor materials, test structures, ageing procedures, filter materials, modulation conditions during sensor operation, etc. for different applications.

- The third approach is chosen by *basic research scientists*, who attempt to identify the atomistic processes of gas sensing. They apply spectroscopies in addition to the phenomenological techniques of sensor characterisation (such as conductivity measurements), perform quantum mechanical calculations, determine simplified models of sensor operation, and aim at the subsequent understanding of thermodynamic or kinetic aspects of sensing mechanisms on the molecular scale. This is usually done on

well-defined model systems for well-defined gas exposures. Consequently this leads to the well-known structural and pressure gaps between the ideal and the real world of surface science.

The present paper aims to bridge the gap between basic and applied research by providing a model description of phenomena involved in the detection process. The models are sensor focussed but are using, to the greatest possible extent, the basic research approach.

The use of the output of these models enables a more specific design of real world sensors.

2. Overview: Contribution of Different Sensor Parts in the Sensing Process and Subsequent Transduction

A sensor element normally comprises the following parts:
- *Sensitive layer* deposited over a
- *Substrate* provided with
- *Electrodes* for the measurement of the electrical characteristics. The device is generally heated by its own
- *Heater*; this one is separated from the *sensing layer* and the *electrodes* by an electrical insulating layer.

Generally the conductance or the resistance of the sensor is monitored as a function of the concentration of the target gases. Additionally the performance of the sensor depends on the
- *Measurement parameters*, such as sensitive layer polarisation or temperature, which are controlled by using different electronic circuits.

The elementary reaction steps of gas sensing will be transduced into electrical signals measured by appropriate electrode structures. The sensing itself can take place at different sites of the structure depending on the morphology. They will play different roles, according to the sensing layer morphology. An overview is given in Fig. 1.

A simple distinction can be made between:
- compact layers; the interaction with gases takes place only at the geometric surface (Fig. 2, such layers are obtained with most of the techniques used for thin film deposition) and
- porous layers; the volume of the layer is also accessible to the gases and in this case the active surface is much higher than the geometric one (Fig. 3, such layers are characteristic to thick film techniques and RGTO (*R*heotaxial *G*rowth and *T*hermal *O*xidation) [1]).

For compact layers, there are at least two possibilities: completely or partly deploted layers, depending on the ratio between layer thickness and Debye length λ_D.
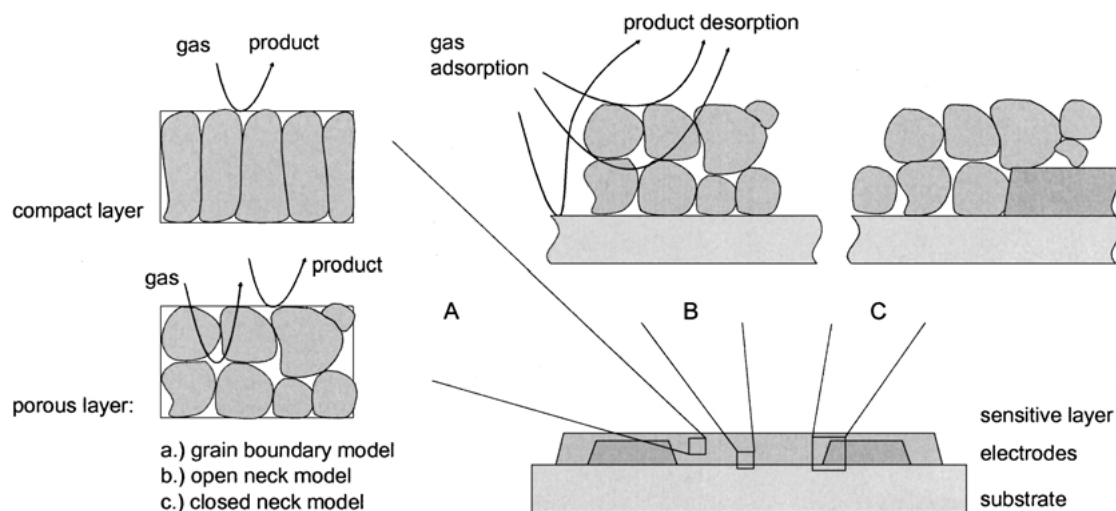

Fig. 1. Schematic layout of a typical resistive gas sensor. The sensitive metal oxide layer is deposited over the metal electrodes onto the substrate. In the case of compact layers, the gas cannot penetrate into the sensitive layer and the gas interaction is only taking place at the geometric surface. In the case of porous layers the gas penetrates into the sensitive layer down to the substrate. The gas interaction can therefore take place at the surface of individual grains, at grain-grain boundaries and at the interface between grains and electrodes and grains and substrates.
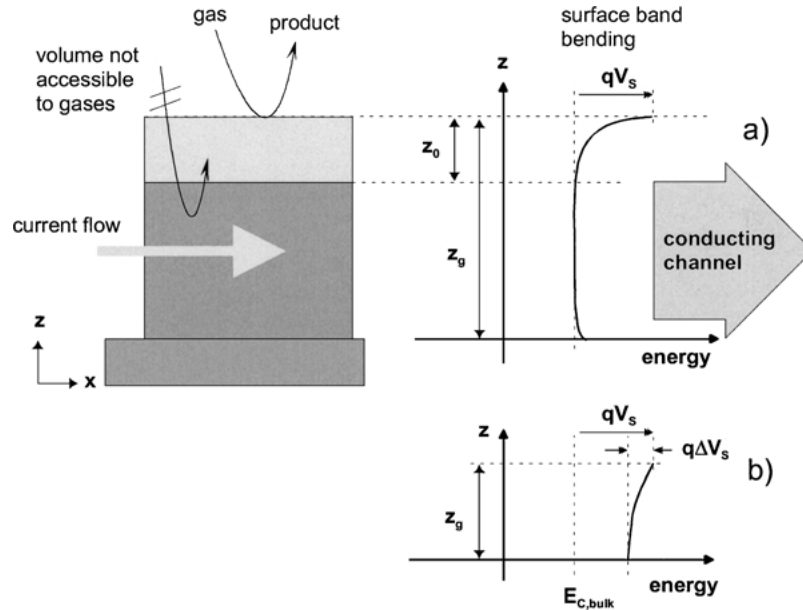
Fig. 2. Schematic representation of a compact sensing layer with geometry and energy band representations; z_0 is the thickness of the depleted surface layer; z_g is the layer thickness and qV_s the band bending. a) represents a partly depleted compact layer ("thicker"), b) represents a completely depleted layer ("thinner"). For details, see text and [17].
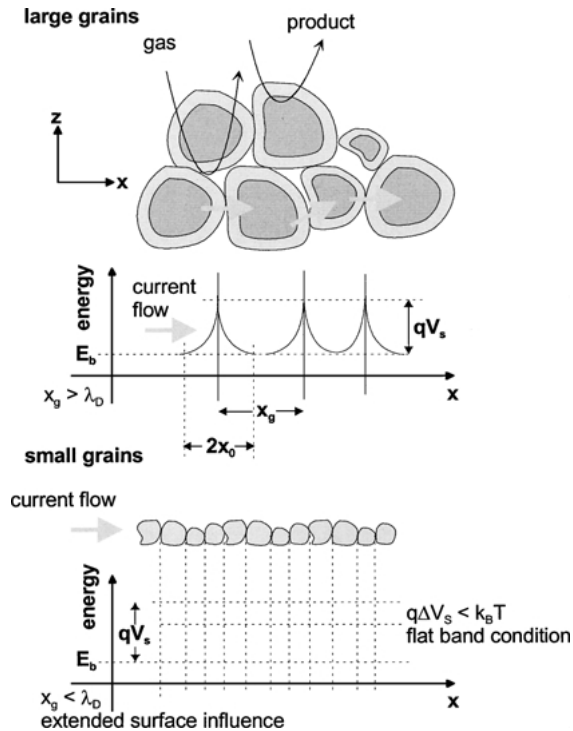

Fig. 3. Schematic representation of a porous sensing layer with geometry and energy band. λ_D Debye length, x_g grain size. For details, see text and [17].

For partlydepleted layers, when surface reactions do not influence the conduction in the entire layer ($z_g > z_0$ see Fig. 2), the conduction process takes place in the bulk region (of thickness $z_g - z_0$, much more conductive that the surface depleted layer). Formally two resistances occur in parallel, one influenced by surface reactions and the other not; the conduction is parallel to the surface, and this explains the limited sensitivity. Such a case is generally treated as a conductive layer with a reaction-dependent thickness. For the case of completely depleted layers in the absence of reducing gases, it is possible that exposure to reducing gases acts as a switch to the partly depleted layer case (due to the injection of additional free charge carriers). It is also possible that exposure to oxidizing gases acts as a switch between partly depleted and completely depleted layer cases.

For porous layers the situation may be complicated further by the presence of necks between grains (Fig. 5). It may be possible to have all three types of contribution presented in Fig. 4 in a porous layer: surface/bulk (for large enough necks $z_n > z_0$, Fig. 5), grain boundary (for large grains not sintered together), and flat bands (for small grains and small necks). Of course, what was mentioned for compact layers, i.e. the possible switching role of reducing gases, is valid also
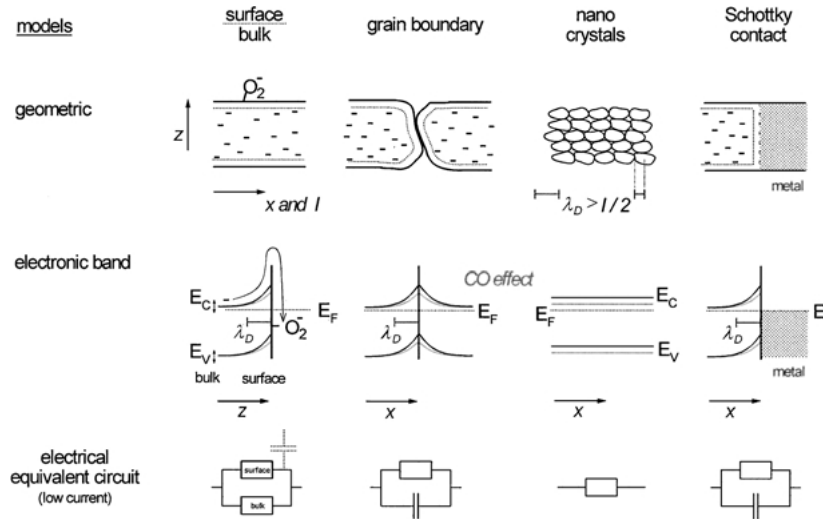
Fig. 4. Different conduction mechanisms and changes upon O_2 and CO exposure to a sensing layer in overview: This survey shows geometries, electronic band pictures and equivalent circuits. E_C minimum of the conduction band, E_V maximum of the valence band, E_F Fermi level, and λ_D Debye length. For details, see text and [18].
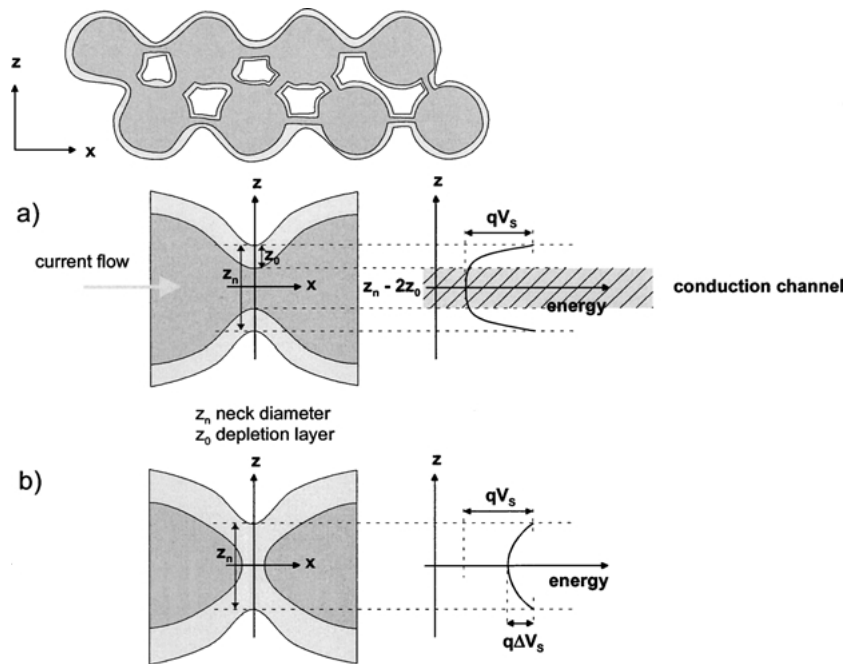

Fig. 5. Schematic representation of a porous sensing layer with geometry and surface energy band-case with necks between grains. z_n is the neck diameter; z_0 is the thickness of the depletion layer. a) represents the case of only partly depleted necks whereas b) represents large grains where the neck contact is completely depleted. For details, see text and [17].

for porous layers. For small grains and narrow necks, when the mean free path of free charge carriers becomes comparable with the dimension of the grains, a surface influence on mobility should be taken into consideration. This happens because the number of collisions experienced by the free charge carriers in the bulk of the grain becomes comparable with the number of surface collisions; the latter may be influenced by
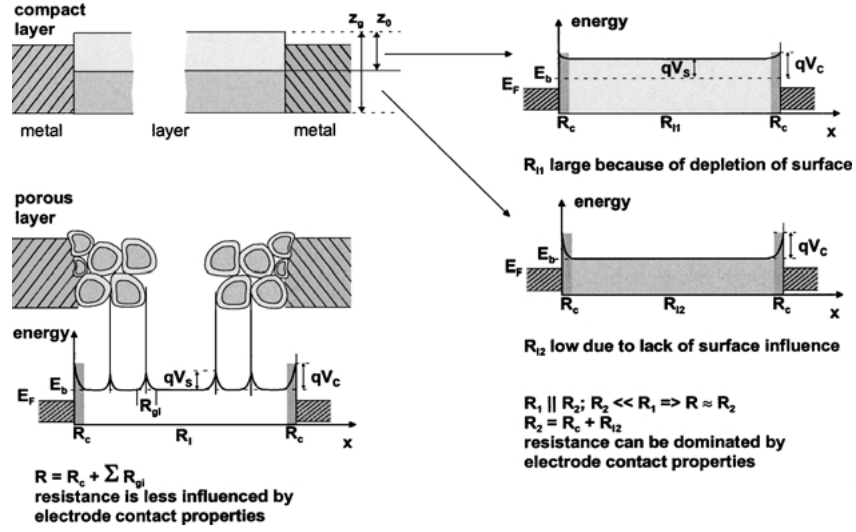
Fig. 6. Schematic representation of compact and porous sensing layers with geometry and energetic bands, which shows the possible influence of electrode-sensing layers contacts. R_C is the resistance of the electrode-SnO$_2$ contact, R_{l1} is the resistance of the depleted region of the compact layer, R_{l2} is the resistance of the bulk region of the compact layer, R_1 is the equivalent series resistance of R_{l1} and R_C, R_2 is the equivalent series resistance of R_{l2} and R_C, R_{gi} is the average intergrain resistance in the case of porous layer, E_b is the minimum of the conduction band in the bulk, $q\,V_S$ is the band bending associated with surface phenomena on the layer, and $q\,V_C$ also contains the band bending induced at the electrode-SnO$_2$ contact.

adsorbed species acting as additional scattering centres (see discussion in [2]).

Figure 6 illustrates the way in which the metal-semiconductor junction, built at electrodesensitive layer interfaces, influences the overall conduction process. For compact layers they appear as a contact resistance (R_C) in series with the resistance of the SnO$_2$ layer. For partly depleted layers, R_C could be dominant, and the reactions taking place at the three-phase boundary, electrode-SnO$_2$-atmosphere, control the sensing properties.

In porous layers the influence of R_C may be minimized due to the fact that it will be connected in series with a large number of resistances, typically thousands, which may have comparable values (R_{gi} in Fig. 6). Transmission line measurements (TLM) performed with thick SnO$_2$ layers exposed to CO and NO$_2$ did not result in values of R_C clearly distinguishable from the noise [3], while in the case of dense thin films the existence of R_C was proved [4]. Again, the relative importance played by different terms may be influenced by the presence of reducing gases due to the fact that one can expect different effects for grain-grain interfaces when compared with electrode-grain interfaces.

3. Influence of Gas Reaction on the Surface Concentration of Free Charge Carriers

In the following, different contributions to the charge carrier concentration, n_S, in the depletion layer at the surface will be described.

3.1. Oxygen

At temperatures between 100 and 500°C the interaction with atmospheric oxygen leads to its ionosorption in molecular (O$_2^-$) and atomic (O$^-$, O^{--}) forms (Fig. 7). It is proved by TPD, FTIR, and ESR that below 150°C the molecular form dominates and above this temperature the ionic species dominate. The presence of these species leads to the formation of a depletion layer at the surface of tin oxide. We will assume that in the cases we are examining, the surface coverage is dominated by one species. The dominating species are depending on temperature and, probably, on surface dopants.

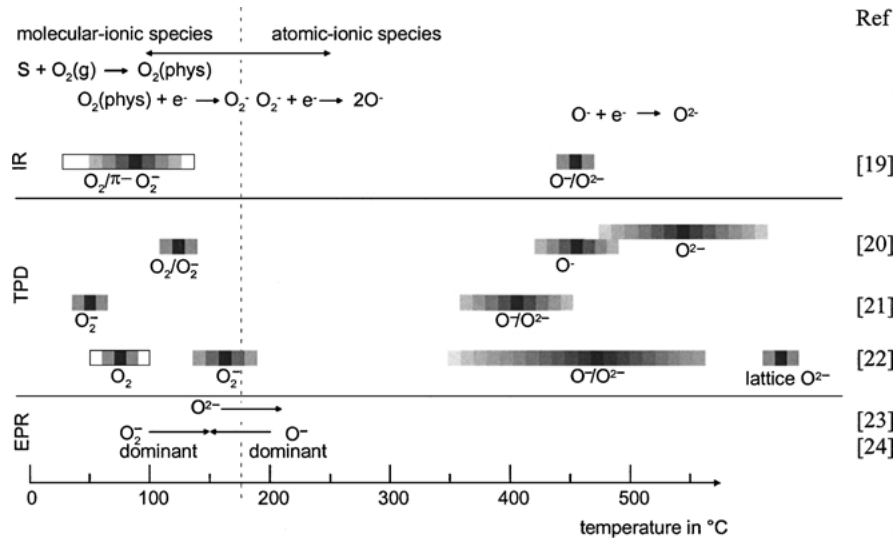The equation describing the oxygen chemisorption can be written as:

$$\frac{\beta}{2}O_2^{gas} + \alpha \cdot e^- + S \rightleftharpoons O_{\beta S}^{-\alpha} \tag{1}$$
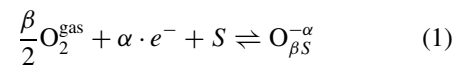
Fig. 7. Literature survey of oxygen species detected at different temperatures at SnO$_2$ surfaces with IR (infrared analysis), TPD (temperature programmed desorption), EPR (electron paramagnetic resonance). For details, see listed references.

where

O_2^{gas} is an oxygen molecule in the ambient atmosphere; e^- is an electron, which can reach the surface that means it has enough energy to overcome the electric field resulting from the negative charging of the surface. Their concentration is denoted n_S; $n_S = [e^-]$; S is an unoccupied chemisorption site for oxygen–surface oxygen vacancies and other surface defects are generally considered candidates; $O_{\beta S}^{-\alpha}$ is a chemisorbed oxygen species with:

$\alpha = 1$ for singly ionised forms
$\alpha = 2$ for doubly ionised form.
$\beta = 1$ for atomic forms
$\beta = 2$ for molecular form

The chemisorption of oxygen is a process that has two parts: an electronic one and a chemical one. This follows from the fact that the adsorption is produced by the capture of an electron at a surface state, but the surface state doesn't exist in the absence of the adsorbed atom/molecule. This fact indicates that at the beginning of the adsorption, the limiting factor is chemical, the activation energy for adsorption/dissociation, due to the unlimited availability of free electrons in the absence of band bending. After the building of the surface charge, a strong limitation is coming from the potential barrier that has to be overcome by the electrons in order to reach the surface. Desorption is controlled, from the very beginning, by both electronic and chemical parts; the activation energy is not changed during the process if the coverage is not high enough to provide interaction between the chemisorbed species [5]. The activation energies for adsorption and desorption are included in the reaction constants, k_{ads} and k_{des}. From Eq. (1) we can deduce using the mass action law:

$$k_{ads} \cdot [S] \cdot n_S^\alpha \cdot p_{O_2}^{\beta/2} = k_{des} \cdot \left[O_{\beta S}^{-\alpha}\right] \qquad (2)$$

$[S_t]$ being the total concentration of available surface sites for oxygen adsorption, occupied or unoccupied. By defining the surface coverage θ with chemisorbed oxygen as:

$$\theta = \frac{\left[O_{\beta S}^{-\alpha}\right]}{[S_t]} \qquad (3)$$

and using the conservation of surface sites:

$$[S] + \left[O_{\beta S}^{-\alpha}\right] = [S_t] \qquad (4)$$

we can write:

$$(1 - \theta) \cdot k_{ads} \cdot n_S^\alpha \cdot p_{O_2}^{\beta/2} = k_{des} \cdot \theta \qquad (5)$$

Equation (5) is giving a relationship between the surface coverage with ionosorbed oxygen and the concentration of electrons with enough energy to reach the surface. If hopping of electrons from one grain to another controls the electrical conduction in the layer, this electron concentration is the one that is participating in conduction. Equation (5) is not enough for finding the relationship between n_S and the concentration of oxygen in the gaseous phase, p_{O_2}, due to the fact that the surface coverage and n_S are related. We need an additional equation and we can use the electroneutrality condition combined with the Poisson equation.

The electroneutrality equation in the Schottky approximation states that the charge in the depletion layer is equal to the charge captured at the surface.

We will consider that we are at temperatures high enough to have all donors ionised (concentration of ionised donors equals the bulk electron density n_b). If one assumes the Schottky approximation to be valid, we will have all the electrons from the depletion layer captured on surface levels.

The following section describes how one obtains the second relation between θ and n_S (the first relation is given in Eq. (5)). The results are valid also in the case where θ is influenced by the presence of additional gases. An example for CO will be provided in Section 3.3.

One can distinguish between two limiting cases:

Case 1. Grains/crystallites large enough to have a bulk region unaffected by surface phenomena ($d \gg \lambda_D$; see 3.1.1)

Case 2. Grains/crystallites smaller than or comparable to $\lambda_D (d \leq \lambda_D$; see 3.1.2)

3.1.1. Large grains. The situation is described by Fig. 8; for large grains, one generally treats the situation in a planar and semi-infinite manner. qV_S is the band bending, z_0 denotes the depth of the depleted region and A the covered area.

In the *first case* (large grains), we can write the electroneutrality (6) and the Poisson equations (7) for energy (E) as:

$$\alpha \cdot \theta \cdot [S_t] \cdot A = n_b \cdot z_0 \cdot A = Q_{SS} \qquad (6)$$

$$\frac{d^2 E(z)}{dz^2} = \frac{q^2 \cdot n_b}{\varepsilon \cdot \varepsilon_0} \qquad (7)$$
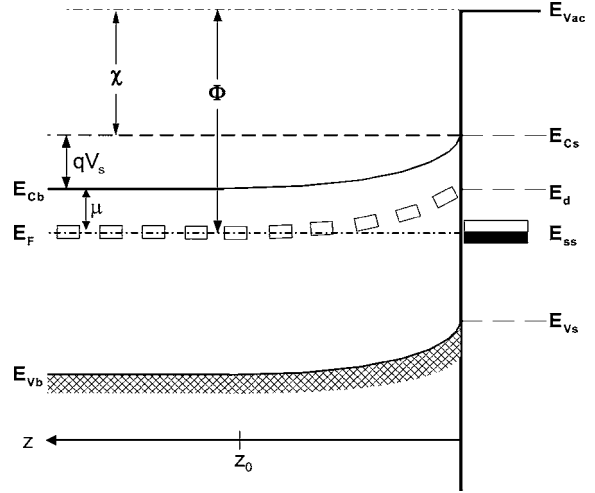

Fig. 8. Band bending after chemisorption of charged species (here ionosorption of oxygen on E_{SS} levels). Φ denotes the work function, χ is the electron affinity, and μ the electrochemical potential.

the boundary conditions for the Poisson equation are

$$\left. \frac{dE(z)}{dz} \right|_{z=z_0} = 0 \qquad (8)$$

$$E(z)|_{z=z_0} = E_C \qquad (9)$$

one obtains from the Poisson equation:

$$E(z) = E_C + \frac{q^2 \cdot n_b}{2 \cdot \varepsilon \cdot \varepsilon_0} \cdot (z - z_0)^2 \qquad (10)$$

which results in the general dependence of band bending, given that $V = E/q$

$$V(z) = \frac{q \cdot n_b}{2 \cdot \varepsilon \cdot \varepsilon_0} \cdot (z - z_0)^2 \qquad (11)$$

and for the surface band bending

$$V_S = \frac{q \cdot n_b}{2 \cdot \varepsilon \cdot \varepsilon_0} \cdot z_0^2 \qquad (12)$$

By combining Eqs. (6) and (12) and using the following relation 13 between V_S and n_S

$$n_s = n_b \exp\left(-\frac{qV_s}{k_B T}\right) \qquad (13)$$

one obtains

$$\theta = \sqrt{\frac{2 \cdot \varepsilon \cdot \varepsilon_0 \cdot n_b \cdot k_B \cdot T}{\alpha^2 \cdot [S_t]^2 \cdot q^2}} \cdot \ln \frac{n_b}{n_S} \qquad (14)$$

which together with Eq. (5) allows the determination of n_S and θ as a function of partial pressures (p_{O_2}), temperature T, ionisation and chemical state of oxygen α, β, reaction constants k_{ads}, k_{des}, material constants ε, n_b, $[S_t]$ and fundamental constants, k_B, ε_0. The latter relation can, for example be solved numerically or by using different approximations.

3.1.2. Small grains. In the *second case* (small grains) it is also important to evaluate the band bending between the surface and the centre of the grain. The following discussion is originally given in [2]:

The calculations assume a conduction taking place in cylindrical filaments (with radius R) obtained by the sintering of small grains. Using this assumption, one can write the Poisson equation in cylindrical coordinates directly for energy E using the Schottky approximation. For the given geometry, the radial part of the Poisson equation is:

$$\left(\frac{1}{r}\frac{d}{dr} + \frac{d^2}{dr^2}\right)E(r) = \frac{q^2 n_b}{\varepsilon \varepsilon_0} \qquad (15)$$

The boundary conditions are:

$$E(r)|_{r=0} = E_0 \qquad (16)$$

$$\left.\frac{dE(r)}{dr}\right|_{r=0} = 0 \qquad (17)$$

Using Eqs. (15)–(17) one obtains for $\Delta E = E(R) - E_0$:

$$\Delta E = \frac{q^2 n_b}{4\varepsilon \varepsilon_0} R^2 \qquad (18)$$

or by using the formula of the Debye length obtained in the Schottky approximation

$$\lambda_D = \sqrt{\frac{\varepsilon \varepsilon_0 k_B T}{q^2 n_b}} \qquad (19)$$

one obtains

$$\Delta E \sim k_B \cdot T \cdot \left(\frac{R}{2 \cdot \lambda_D}\right). \qquad (20)$$

Table 1. Bulk and surface parameters of influence for SnO_2 single crystals. n_b is the concentration of free charge carriers (electrons), μ_b is their Hall mobility, λ_D is the Debye length, and λ is the mean free path of free charge carriers (electrons).

T(K)	400	500	600	700
n_b (10^{19})	1	11	58	260
μ_b (10^{-4} m^2/(Vs))	178	87	49	31
λ_D (nm)	129	43	21	11
λ (nm)	1.96	1.07	0.66	0.45
$\Delta E/(k_B T)|_{(R=50\ nm)}$	0.34	0.77	1.08	1.49

If ΔE is comparable with the thermal energy, this leads to a homogeneous electron concentration in the grain and in turn to the flat band case. One can show that, using data available in the literature (see [2] and Table 1), for grain sizes lower than 50 nm, complete grain depletion and a flat band condition can be accepted almost for all relevant temperatures (excluding e.g. 700 K since the value of ΔE is larger than $k_B T$).

The electroneutrality condition now takes the form (in flat band condition)

$$\alpha \cdot \theta \cdot [S_t] \cdot A + n_S \cdot V = n_b \cdot V \qquad (21)$$

where n_S is now the homogenous concentration of electrons throughout the whole tin oxide crystallites as illustrated in Fig. 4.

Assuming that the cylinder length is L, having in mind the surface A of a cylinder as

$$A = 2 \cdot \pi \cdot R \cdot (R + L) \qquad (22)$$

and the volume V as

$$V = \pi \cdot R^2 \cdot L \qquad (23)$$

and combining Eqs. (21)–(23)

$$\theta = \frac{n_b \cdot R}{2 \cdot \alpha \cdot [S_t] \cdot \left(1 + \frac{R}{L}\right)} \cdot \left(1 - \frac{n_S}{n_b}\right) \qquad (24)$$

With the approximation of R/L close to zero one obtains

$$\theta = \frac{n_b \cdot R}{2 \cdot \alpha \cdot [S_t]} \cdot \left(1 - \frac{n_S}{n_b}\right) \qquad (25)$$

This together with Eq. (5) allows the determination of n_S and θ as a function of only partial pressures (p_{O_2}), temperature T, ionisation and chemical state of oxygen α, β, reaction constants k_{ads}, k_{des}, material constants n_b, $[S_t]$ and fundamental constant k_B. The latter relation can be, for example, solved numerically or by using different approximations.

3.2. Water Vapour

At temperatures between 100 and 500°C, the interaction with water vapour leads to molecular water and hydroxyl groups adsorption (Fig. 9). Water molecules can be adsorbed by physisorption or hydrogen bonding. TPD and IR studies show that at temperatures above 200°C, molecular water is no more present at the surface. Hydroxyl groups can appear due to an acid/base reaction with the OH sharing its electronic pair with the Lewis acid site (Sn) and leaving the hydrogen atom ready for reaction maybe with the lattice oxygen, (Lewis base), or with adsorbed oxygen. IR studies are indicating the presence of hydroxyl groups bound to Sn atoms.

There are three types of mechanisms explaining the experimentally proven increase of surface conductivity in the presence of water vapour. Two, direct mechanisms are proposed by Heiland and Kohl [6] and the third, indirect, is suggested by Morrison and by Henrich and Cox [5, 7].

The *first mechanism* of Heiland and Kohl attributes the role of electron donor to the 'rooted' OH group, the one including lattice oxygen. The equation proposed is:

$$H_2O^{gas} + Sn_{Sn} + O_O$$
$$\rightleftharpoons (Sn_{Sn}^+ - OH^-) + (OH)_O^+ + e^- \qquad (26)$$
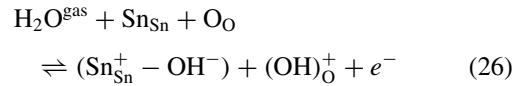
Where $(Sn_{Sn}^+ - OH^-)$ is denominated as an isolated hydroxyl or OH group and $(OH)_O^+$ is the rooted one. In the upper equation, the latter is already ionised.

The reaction implies the homolytic dissociation of water and the reaction of the neutral H atom with the lattice oxygen. The latter is normally in the lattice fixing two electrons consequently being in the 2-state. The built up rooted OH group, having a lower electron affinity and consequently can get ionised and become a donor (with the injection of an electron in the conduction band).

The *second mechanism* takes into account the possibility of the reaction between the hydrogen atom and the lattice oxygen and the binding of the resulting hydroxyl group to the Sn atom. The resulting oxygen
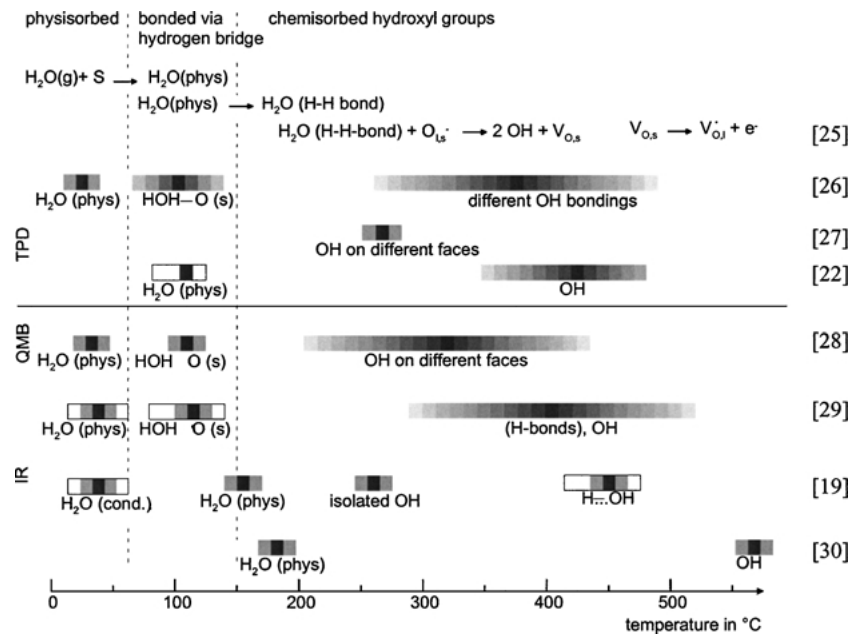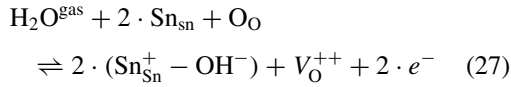

Fig. 9. Literature survey of water-related species formed at different temperatures at SnO$_2$ surfaces. For details, see listed references.

vacancy will produce, by ionisation, the additional electrons. The equation proposed by Heiland and Kohl [6] is:

$$H_2O^{gas} + 2 \cdot Sn_{sn} + O_O$$
$$\rightleftharpoons 2 \cdot (Sn^+_{Sn} - OH^-) + V^{++}_O + 2 \cdot e^- \quad (27)$$

Morrison, as well as Henrich and Cox [5, 7], consider an indirect effect more probable. This effect could be the interaction between either the hydroxyl group or the hydrogen atom originating from the water molecule with an acid or basic group, which are also acceptor surface states. Their electronic affinity could change after the interaction. It could also be the influence of the co-adsorption of water on the adsorption of another adsorbate, which could be an electron acceptor. Henrich and Cox suggested that the pre-adsorbed oxygen could be displaced by water adsorption. In any of these mechanisms, the particular state of the surface has a major role, due to the fact that it is considered that steps and surface defects will increase the dissociative adsorption. The surface dopants could also influence these phenomena; Egashira et al. [8] showed by TPD and isotopic tracer studies combined with TPD that the oxygen adsorbates are rearranged in the presence of adsorbed water. The rearrangement was different in the case of Ag and Pd surface doping.

In choosing between one of the proposed mechanisms, one has to keep in mind that:

- in all reported experiments, the effect of water vapour was the increase of surface conductance,
- the effect is reversible, generally with a time constant in the range of around 1 h.

It is not easy to quantify the effect of water adsorption on the charge carrier concentration, n_S (which is normally proportional to the measured conductance). For the first mechanism of water interaction proposed by Heiland and Kohl ("rooted", Eq. (26)), one could include the effect of water by considering the effect of an increased background of free charge carriers on the adsorption of oxygen (e.g. in Eq. (1)).

For the second mechanism proposed by Heiland and Kohl ("isolated", Eq. (27)) one can examine the influence of water adsorption (see [9]) as an electron injection combined with the appearance of new sites for oxygen chemisorption; this is valid if one considers oxygen vacancies as good candidates for oxygen adsorption. In this case one has to introduce the change

in the total concentration of adsorption sites $[S_t]$:

$$[S_t] = [S_{t0}] + k_0 \cdot p_{H_2O} \quad (28)$$

obtained by applying the mass action law to Eq. (27). $[S_{t0}]$ is the intrinsic concentration of adsorption sites and k_0 is the adsorption constant for water vapour. One will have to correct also the electroneutrality equation and the result of the calculations indicate for the case of large grains and O^{2-} as dominating oxygen species [9]:

$$n_S^2 \sim p_{H_2O} \quad (29)$$

In the case of the interaction with surface acceptor states, not related to oxygen adsorption, we can proceed as in the case of the first mechanism proposed by Kohl. In the case of an interaction with oxygen adsorbates, we can consider that k_{des}, Eq. (2), is increased.

3.3.   CO

Carbon monoxide is considered to react, at the surface of oxides, with pre-adsorbed or lattice oxygen (Henrich and Cox) [7]. IR studies identified CO related species:
- unidentate and bidentate carbonate between 150°C and 400°C,
- carboxylate between 250°C and 400°C.

By FTIR the formation of CO_2 as a reaction product was identified between 200°C and 370°C (Lenaerts) [10].

In all experimental studies (Fig. 10), in air at temperatures between 150°C and 450°C, the presence of CO increased the surface conduction. A simple model adds to Eq. (1) the following equation:

$$\beta \cdot CO^{gas} + O^{-\alpha}_{\beta S} \rightarrow \beta \cdot CO_2^{gas} + \alpha \cdot e^- + S \quad (30)$$

and the rate equation for the oxygen surface coverage will be, by combining Eqs. (1) and (30):

$$\frac{d[O^{-\alpha}_{\beta S}]}{dt} = \underbrace{k_{ads} \cdot [S] \cdot n_S^\alpha \cdot p_{O_2}^{\beta/2} - k_{des} \cdot [O^{-\alpha}_{\beta S}]}_{\text{related to ad−and desorption of oxygen}}$$
$$\underbrace{-k_{react} \cdot p_{CO}^\beta [O^{-\alpha}_{\beta S}]}_{\text{related to CO reaction}} \quad (31)$$

where k_{reac} is the reaction constant for carbon dioxide production. One also considers that the concentration
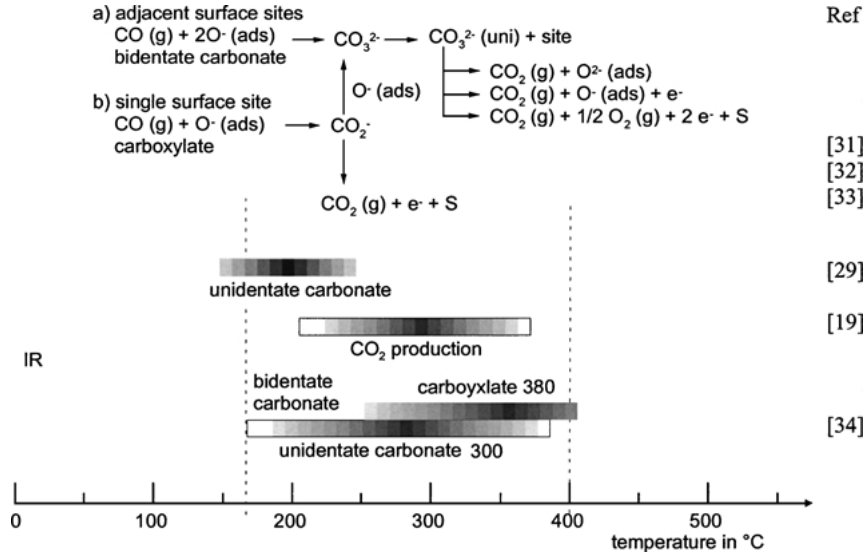
Fig. 10. Literature survey of species found as a result of CO adsorption at different temperatures on a (O_2) preconditioned SnO_2 surface. For details, see listed references.

of CO reacting at the surface is proportional with the concentration in the gaseous phase. This assumption should work at the CO concentrations in air (ppm) for which detection is interesting.

In the case of steady state, using the definition for the surface coverage (Eq. (3)), the conservation of surface sites (Eq. (4)) and dividing Eq. (31) by $[S_t]$ one obtains

$$k_{ads} \cdot (1 - \theta) \cdot n_S^\alpha \cdot p_{O_2}^{\beta/2} = \left(k_{des} + k_{react} \cdot p_{CO}^\beta\right) \cdot \theta \quad (32)$$

Equation (32) is the equivalent of Eq. (5) for the case where, in addition to oxygen, a reducing gas (namely CO) is also present. At this point, one has to discuss again the two cases of large and small crystallites discussed earlier (see Section 3.1).

3.3.1. Large grains. For the *first case*, the electroneutrality condition is still described by the following Eq. (14):

$$\theta = \sqrt{\frac{2 \cdot \varepsilon \cdot \varepsilon_0 \cdot n_b \cdot k_B \cdot T}{\alpha^2 \cdot [S_t]^2 \cdot q^2} \cdot \ln \frac{n_b}{n_S}}$$

or by simple substitution with

$$\theta = \underbrace{\sqrt{\frac{2 \cdot \varepsilon \cdot \varepsilon_0 \cdot n_b \cdot k_B \cdot T}{\alpha^2 \cdot [S_t]^2 \cdot q^2}}}_{\Omega} \cdot \sqrt{\ln \frac{n_b}{n_S}} = \Omega \cdot \sqrt{\ln \frac{n_b}{n_S}}$$

one obtains from Eqs. (14) and (32)

$$\underbrace{\frac{k_{ads}}{k_{des}} \cdot p_{O_2}^{\beta/2} \left(\frac{1}{\Omega \cdot \sqrt{\ln \frac{n_b}{n_S}}} - 1 \right) \cdot n_S^\alpha}_{\omega \cdot n_S^\delta} = 1 + \frac{k_{reac}}{k_{des}} \cdot p_{CO}^\beta$$

$$(33)$$

The logarithmic term in Eq. (33) (left side) has a smaller contribution when compared to n_S^α. It can be shown numerically for values of the parameters relevant to the application (e.g. temperature between 400 and 700 K) that the curly bracket can be approximated by the given function. The values of δ are typically in the range between 0 and 0.2. Accordingly one can rewrite Eq. (33) as

$$\omega \cdot n_S^{(\alpha+\delta)} = 1 + \frac{k_{reac}}{k_{des}} \cdot p_{CO}^\beta \quad (34)$$

3.3.2. Small grains. For the *second case* the electroneutrality condition is still described by the following Eq. (25):

$$\theta = \frac{n_b \cdot R}{2 \cdot \alpha \cdot [S_t]} \cdot \left(1 - \frac{n_S}{n_b}\right)$$

In Eq. (32), one has to deal with θ and $(1 - \theta)$. One can see in Eq. (25) that a variation of n_S will not change θ too much keeping in mind $n_S \ll n_b$. At the same time,

the changes in $(1 - \theta)$ can be important and consequently influence the overall behaviour describing the equation. This can be shown for example for the case described in [2] where the reasons for the following approximation were described:

$$\theta \approx \left(1 - \frac{n_S}{n_b}\right) \qquad (35)$$

Using Eqs. (32) and (35) one obtains the following equation:

$$k_{ads} \cdot \left(1 - \left(1 - \frac{n_S}{n_b}\right)\right) \cdot n_S^\alpha \cdot p_{O_2}^{\beta/2}$$
$$= \left(k_{des} + k_{react} \cdot p_{CO}^\beta\right) \cdot 1 \qquad (36)$$

which can be easily transformed

$$\underbrace{\frac{k_{ads}}{k_{des}} \cdot \frac{p_{O_2}^{\beta/2}}{n_b}}_{\omega'} \cdot n_S^{(\alpha+1)} = 1 + \frac{k_{react}}{k_{des}} \cdot p_{CO}^\beta \qquad (37)$$

and

$$\omega' \cdot n_S^{(\alpha+1)} = 1 + \frac{k_{react}}{k_{des}} \cdot p_{CO}^\beta \qquad (38)$$

3.3.3. Summary. To summarize, one obtains, for the two cases (as discussed above), a different power law dependency:

First case (large grains); one obtains from Eq. (34)

$$n_S = \left(\frac{1}{\omega}\left(1 + \frac{k_{reac}}{k_{des}} \cdot p_{CO}^\beta\right)\right)^{\frac{1}{\alpha+\delta}}$$

which, in the case of large CO concentrations or very sensitive sensors (large k_{reac}),

$$\frac{k_{reac}}{k_{des}} \cdot p_{CO}^\beta \gg 1$$

which leads to

$$n_S \sim p_{CO}^{\frac{\beta}{\alpha+\delta}} \qquad (39)$$

and for the *second case* (small grains) the resulting equation from (38) will be

$$n_S \sim p_{CO}^{\frac{\beta}{\alpha+1}} \qquad (40)$$

The following table gives an overview of the different cases discussed above.

4. Conduction in the Sensing Layer

As stated in the introduction, the relationship between the surface band bending and the measured resistance/conductance of the sensitive layer depends on the morphology of the layer. The first distinction to be made is between porous and compact layers (Fig. 1).

4.1. Compact Layers

In the case of *compact layers*, the active surface is the geometric one and the electrical conduction is taking place in a direction parallel to the maximum effect on the band bending (Fig. 2). When discussing the conductance G, one has to start with the microscopic conductivity σ. Keeping in mind that SnO_2 is an n-type semiconductor, it makes sense to refer to the electronic part of the overall conductivity/conductance.

The electronic conductivity in a homogenous ideal single crystal is given by the following equation:

$$\sigma_b = q \cdot n_b \cdot \mu_b \qquad (41)$$

where the index b is denoting the bulk value (all surface effects are omitted in this case, indicating all values are bulk values), q gives the elementary charge, n the charge carrier/electron concentration and μ the electron mobility. In the case of an *n*-type semiconductor, the relation between the conductivity σ and the conductance G is given by a simple relation (keeping in mind that one is still omitting the surface phenomena) shown in the following:

$$G = const \cdot q \cdot n_b \cdot \mu_b \qquad (42)$$

The constant const includes the geometry of the sample.

By including the surface effects (as presented in Fig. 2), the situation gets a little bit more complicated: The conductivity now depends on the depth z.

$$\sigma(z) = q \cdot n(z) \cdot \mu(z) \qquad (43)$$

For the conductance, one has to integrate over the entire thickness z_g:

$$G = const \cdot \frac{q}{z_g} \int_0^{z_g} n(z) \cdot \mu(z)\, dz \qquad (44)$$

Equation (44) describes the general case of a single crystal or compact layer. One can evaluate, in a simpler manner, the particular cases that are of practical interest.

Specifically, one can distinguish by referring to λ_D between
- relatively thick layers (*first case* $d \gg \lambda_D$) and
- relatively thin layers (*second case* $d \approx \lambda_D$)

4.1.1.   Thick layers.   Here the layer is thick enough to have a region unaffected by surface effects, $d \gg \lambda_D$, so that the majority of conduction will take place in that region; the concentrations of electrons taking part in conduction is, in this case, n_b. The influence of surface phenomena will consist in the modulation of the thickness of this conducting channel. The conductance of the layer can be written (by neglecting conduction in the depleted layer) as:

$$G = \text{const} \cdot (z_g - z_0) \qquad (45)$$

where the constant includes the geometrical factors and the mobility, z_g is the thickness of the layer and z_0 is the depth of the depletion layer. For z_0 one has, in the Schottky approximation, a simple relationship with V_S/n_S (see Eqs. (12), (13) and (39)). Accordingly one has:

$$z_0 = \sqrt{\frac{2 \cdot \varepsilon \cdot \varepsilon_0}{q \cdot n_b} \cdot V_S} \qquad (46)$$

$$\text{const}' \cdot p_{\text{CO}}^{\frac{\beta}{\alpha+\delta}} = n_b \exp\left(-\frac{q V_s}{k_B T}\right) \qquad (47)$$

$$z_0 = \frac{1}{q}$$
$$\cdot \sqrt{2 \cdot \varepsilon \cdot \varepsilon_0 \cdot k_B \cdot T \cdot \ln \frac{n_b}{\text{const}'} - \frac{\beta \cdot k_B \cdot T}{\alpha + \delta} \cdot \ln p_{\text{CO}}}$$
$$(48)$$

and the dependence of conductance on partial pressure of CO will look like, with obvious notations:

$$G = \text{const1} - \sqrt{\text{const2} - \text{const3} \cdot \ln p_{\text{CO}}} \qquad (49)$$

Equation (49) shows the dependency of the measured conductance G on the partial pressure of CO for a compact layer with a thickness larger than λ_D. One can see that, as expected, the dependence of G is extremely

weak on p_{CO} (much weaker than the dependence of n_S on p_{CO}; see Eq. (39)).

4.1.2.   Thin layers.   In the case of thin layers, the thickness of the layer is comparable to λ_D, the influence of surface phenomena is extended to the whole layer (see Fig. 2 lower part). This means that the layer can't be divided into a conducting channel (electron concentration n_b) and a resistive one. The conductance will be related to a concentration of electrons influenced by the surface reactions.
- *Case* (*a*) is the simple one in which the band bending between the surface and the bottom of the layer is comparable with the thermal energy ($e\Delta V_S \leq k_B T$); this means that the concentration of electrons in the whole layer is homogeneous, equal to n_S. The conductance is proportional to n_S and, for the dependence on p_{CO}, one has to use Eq. (40) (thin layer is comparable to small grains). The result is:

$$G \sim p_{\text{CO}}^{\frac{\beta}{\alpha+1}} \qquad (50)$$

- In *case* (*b*), in which the band bending between the surface and the bottom of the layer is higher than the thermal energy ($e\Delta V_S > k_B T$), one has to deal with an average electron concentration; the conductance will be proportional to this average electron concentration, which will have a dependence on p_{CO} closer to the case described by Eq. (39) (large grains). From the practical point of view, one has a dependency of the conductance on p_{CO}:

$$G \sim p_{\text{CO}}^{\frac{\beta}{\alpha+\delta}} \qquad (51)$$

with a value of δ changing from small values to 1. The evaluation of experimentally obtained relationships between conductance/resistance and concentration of test gases should be examined with care; it is not easy to distinguish between a power law dependence and a logarithmic one if the concentration range is not broad enough.

In addition to λ_D there is another "length" which can play a role in the case of narrow layers. This length is the mean free path of electrons, λ. Literature values are provided in Table 1. The importance of this parameter comes from the fact that the ratio z_g/λ gives the weight of surface scattering in the charge carriers' mobility. If the ratio is not too high, the surface scattering can contribute in a significant way to the mobility. Due

to the fact that surface scattering could be influenced by the absorbed species, they could also influence the mobility. An example for the evaluation of the influence of surface phenomena on mobility will be provided for porous layers.

4.2.   Porous Layers

4.2.1.   General discussion.   In the case of *porous layers*, the active surface is much higher than the geometric one (Fig. 3). As presented in detail in the following, the charge carrier transport from one grain to the other is either controlled by

- the (inner) surface barriers (see Fig. 3) or
- very similar to the ones described in relation to compact layers (see Fig. 5).

The layers controlled by the inner surface barriers (see Fig. 3) can be classified according to the dimensions of the grains if it is technologically possible to control the grain size distribution. If such a classification is possible, the results of the modelling already performed for n_S can be applied to the whole layer.

4.2.2.   Large grains.   For large grains, one has to discuss the mechanism of transport of electrons from one grain to the next. This transport mechanism depends on the actual morphology of the grain-grain contact region. One can distinguish between the following three cases:

- *case a)* in which the contact region between grains is small enough ($z_n \ll \lambda_D$) so the charge carriers (electrons from the bulk n_b) will see only one value of V_S when moving from one grain to the other (see Fig. 3 upper part). In this case, the relationship between the conductance and the surface concentration of electrons n_S, the latter given by Eq. (39), depends on the mechanism which describes the transport of the electrons from one grain to the other.
- *case b)* in which the contact region between grains is large but entirely influenced by surface phenomena (closed necks, Fig. 5(b), z_n comparable to λ_D). One has to deal with an averaging of the potential barrier between grains in the case where $q \Delta V_S > k_B T$. That means that the electrons passing from one grain to the other will feel different values of the barrier height depending on their z position (see Fig. 5(b)). One can treat this by considering an effective value of the potential barrier $V_{S,\text{effective}}$ which, for simplicity, one

can consider to have the same dependence on p_{CO} like V_S. When $q \Delta V_S \leq k_B T$, the electrons passing from one grain to the other will all feel the same value of the barrier height V_S. This is equivalent to the case described in the above paragraph.

- *case c)* in which the contact region between grains is large enough ($z_n \gg \lambda_D$) to permit the existence of a region unaffected by surface phenomena (open necks Fig. 5(a)). In this case, one obtains for conductance the same results as for compact layers thicker than λ_D (see compact layer, first case above).

For the first two cases (a and b) described above, one has to examine two different transport mechanisms:

- Diffusion Theory
- Thermoelectronic Emission Theory

These two models will be discussed in subsequent sections

4.2.2.1.   Diffusion theory.   According to [11], if the barrier width $2 \cdot x_0$ is much larger than the mean free path of the electrons λ ($\lambda \ll 2 \cdot x_0$), the current density j is given by

$$j = \sigma(x) \cdot \left(-\frac{dV(x)}{dx} \right) + q \cdot D \cdot \left(\frac{dn(x)}{dx} \right) \quad (52)$$

where $V(x)$ represents the electrostatic potential and $n(x)$ the electron density at the distance x from the interface. $\sigma(x)$ is the local conductivity (see Eq. (41)) and

$$D = k_B \cdot T \cdot \frac{\mu_b}{q} \quad (53)$$

as the carrier diffusion coefficient, where μ_b is the carrier/electron mobility in the bulk and q is the elementary charge. The value of the mobility in Eq. (53) is the bulk one, since the depletion in charge carriers has no effect on the mobility, μ_b. The latter is influenced just by the additional surface scattering effects which are negligible as shown by Eq. (67) (where in fact $r = x_0$). After integration of Eq. (52), one obtains, in the case of zero bias, the following formula for the conductance G. (For details see [12] and the references given in there). One has to keep in mind that this formula only holds if $q \cdot V_S$ is at least several times $k_B \cdot T$. In this case the Fermi-Dirac distribution replacement by the Boltzmann distribution is valid for all respective band bendings $q \cdot V_S$. This limits the applicability of the formula to cases where, even with exposure to reducing gases, the band bending remains

considerable.

$$G_{\text{diff}} = \text{area} \cdot \left(\frac{q^2 \cdot n_b \cdot \mu_b}{k_B \cdot T} \right) \cdot \sqrt{\frac{q \cdot n_b \cdot V_S}{2 \cdot \varepsilon}}$$
$$\cdot \exp\left(-\frac{qV_S}{k_B \cdot T} \right) \tag{54}$$

The *area* in Eq. (54) is a constant with the dimension of m^2 and represents the effective area seen by the electrons while travelling from one grain to the other. One has to remember that V_S is the equilibrium barrier height. The zero bias condition holds in almost all of the later given experimental cases since the measurement potential is very small (typically 100 mV) and distributed across all grain-grain boundaries.

In this case, the relation between G_{diff} (Eq. (54)) and n_S (Eq. (13)) is not linear which means that by measuring the resistance one cannot get directly to the dependence on the surface charge carriers n_S.

4.2.2.2. Thermoelectronic emission theory. The thermoelectronic emission theory applies for the case in which the mean free path of the electrons $\lambda \geq 2 \cdot x_0$ (which is the depletion/barrier width). According to this model, only those among the carriers that possess a kinetic energy larger than the barrier height can move across the boundary. The net current is proportional to the difference of the electron fluxes crossing the boundary from left to right and from right to left, respectively [13]:

$$j = q \cdot n_b \cdot \tilde{v}_{\text{th}} \cdot \left(\exp\left(-\frac{q \cdot V_{S2}}{k_B \cdot T} \right) \right.$$
$$\left. - \exp\left(-\frac{q \cdot V_{S1}}{k_B \cdot T} \right) \right) \tag{55}$$

where

$$\tilde{v}_{\text{th}} = \sqrt{\frac{8 \cdot k_B \cdot T}{\pi \cdot m^*}} \tag{56}$$

is the mean thermal velocity of the carriers (effective mass m^*) in the direction normal to the interface. V_{S1} and V_{S2} are the respective barrier heights under a bias U ($U = V_{S2} - V_{S1}$). The zero bias conductance is:

$$G_{\text{thermo}} = \text{area}' \cdot \left(\frac{q}{k_B \cdot T} \right) \cdot q \cdot n_b \cdot \tilde{v}_{\text{th}}$$
$$\cdot \exp\left(-\frac{qV_S}{k_B \cdot T} \right) \tag{57}$$

Table 2. Summary table of different cases discussed in this section.

Reactive oxygen species	α	β	Large grains	Small grains
O_2^-	1	2	$n_S \sim p_{\text{CO}}^{\frac{2}{1+\delta}}$	$n_S \sim p_{\text{CO}}$
O^-	1	1	$n_S \sim p_{\text{CO}}^{\frac{1}{1+\delta}}$	$n_S \sim p_{\text{CO}}^{0.5}$
O^{--}	2	1	$n_S \sim p_{\text{CO}}^{\frac{1}{2+\delta}}$	$n_S \sim p_{\text{CO}}^{0.33}$

The area' in Eq. (57) is again a constant with the dimension of m^2 and represents the effective area seen by the electrons while travelling from one grain to the other.

Comparing the formula for G_{thermo} (Eq. (57)) with the relation between V_S and n_S (Eq. (13)) one can conclude that G_{thermo} is linear proportional with n_S.

$$G_{\text{thermo}} \sim n_S \tag{58}$$

Accordingly, the power law dependence of n_S on the reducing gas concentration can be directly monitored by measuring the resistance (see Table 2).

4.2.2.3. Conclusion. The main difference between the two mechanisms (diffusion theory or thermoelectronic emission) as given by Eqs. (54) and (57), besides the constants, is the additional dependency on the square root of V_S in the diffusion case.

In order to evaluate the differences between the two models, one has to compare the sensor signal S. The latter is defined as the ratio of two conductance values and using it has the advantage of eliminating the non-relevant terms. One has to focus on the following considerations:

For the *Diffusion Theory*, G_{diff} in air is denoted as $G_{\text{diff},0}$:

$$G_{\text{diff},0} \sim \sqrt{V_{S,0}} \cdot \exp\left(-\frac{q \cdot V_{S,0}}{k_B \cdot T} \right) \tag{59}$$

and G_{diff} in e.g. CO is denoted as $G_{\text{diff},\text{CO}}$:

$$G_{\text{diff},\text{CO}} \sim \sqrt{V_{S,\text{CO}}} \cdot \exp\left(-\frac{q \cdot V_{S,\text{CO}}}{k_B \cdot T} \right) \tag{60}$$

one obtains for the sensor signal S_{Diff}:

$$S_{\text{Diff}} = \frac{G_{\text{diff},\text{CO}}}{G_{\text{diff},0}} = \sqrt{1 - \frac{\Delta V_S}{V_{S,0}}} \cdot \exp\left(-\frac{q \cdot \Delta V_S}{k_B \cdot T} \right) \tag{61}$$

with

$$\Delta V_S = V_{S,0} - V_{S,\text{CO}} \tag{62}$$

which is under reducing conditions always positive since the band bending is reduced.

Applying the same formalism to the *Thermoelectric Emission Theory*, one gets the following relation

$$S_{\text{Thermo}} = \exp\left(\frac{q \cdot \Delta V_S}{k_B \cdot T}\right) \tag{63}$$

The *difference* between these two models in relation to the sensor signal ΔS is consequently:

$$\Delta S = S_{\text{Thermo}} - S_{\text{Diff}}$$
$$= \exp\left(\frac{q \cdot \Delta V_S}{k_B \cdot T}\right) \cdot \underbrace{\left(1 - \sqrt{1 - \frac{\Delta V_S}{V_{S,0}}}\right)}_{\textit{difference}} \tag{64}$$

In order to show the differences between those two models a calculation was performed which results in plots displayed in Figs. 11 and 12. The boundary conditions for the calculation are as follows:

- The validity of both models is ensured by an initial band bending which exceeds a few $k_B T$ (the latter allowing the replacement of the Fermi-Dirac distribution by the Boltzmann one). The upper limit of the initial band bending in accordance with e.g.

Morrison [5] is considered in the calculation to be 1 eV. The lower limit was assumed to be 0.5 eV.
- The temperature was fixed to 300°C, which is a typical temperature for a SnO$_2$ sensor.
- The maximum sensor signal S was considered to be 100 for the Thermoelectronic Emission Theory case. This results, according to Eq. (63), in a maximum change of band bending $q \, \Delta V_S$ of 0.227 eV. The starting point for the change of band banding is of course 0 eV.

The resulting three-dimensional surfaces are:
- in Fig. 11 the sensor signal of the Diffusion Theory model; the Thermoelectronic Emission Theory is independent of the initial band bending and therefore is shown here only as a solid black line
- in Fig. 12 what is described as "*difference*" in Eq. (64), expressed in%.

As shown by the calculation, at relatively high initial band bandings and for sensor signals S lower than e.g. 20 the differences between the two models are not important.

As stated in Eq. (58) there is a linear relation between G and n_S in the case of the Thermoelectronic Emission. Since the difference between the two models is not important, a general applicability of the linear relation is possible for lower sensor signals.

At higher sensor signals S, the difference between the two models becomes considerable. Nevertheless, there is a possibility to link in a simple manner both conductance models to n_S. By numerical evaluation of
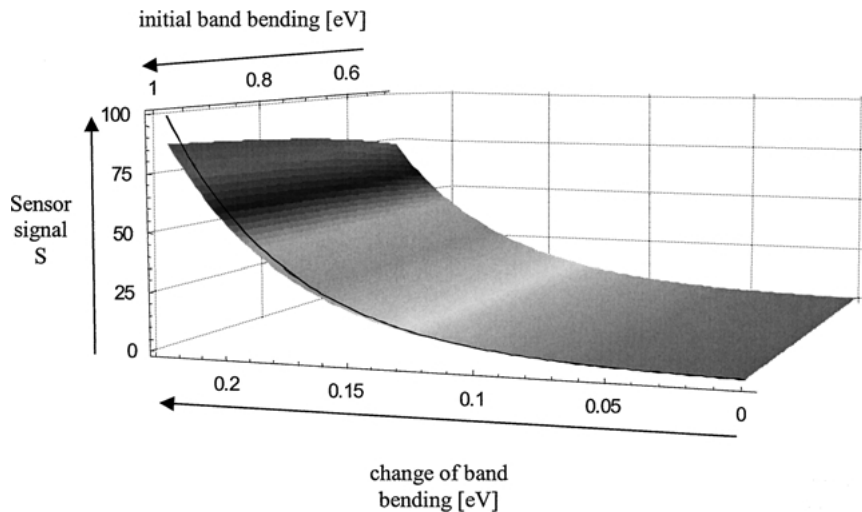

Fig. 11. Sensor Signal *S* for the Thermoelectronic Emission Theory (solid black line) and Diffusion theory (shaded 3D-plot) as a function of the initial band bending $V_{S,0}$ and the change in the band bending ΔV_S. The boundary conditions for the calculation are given in the text.
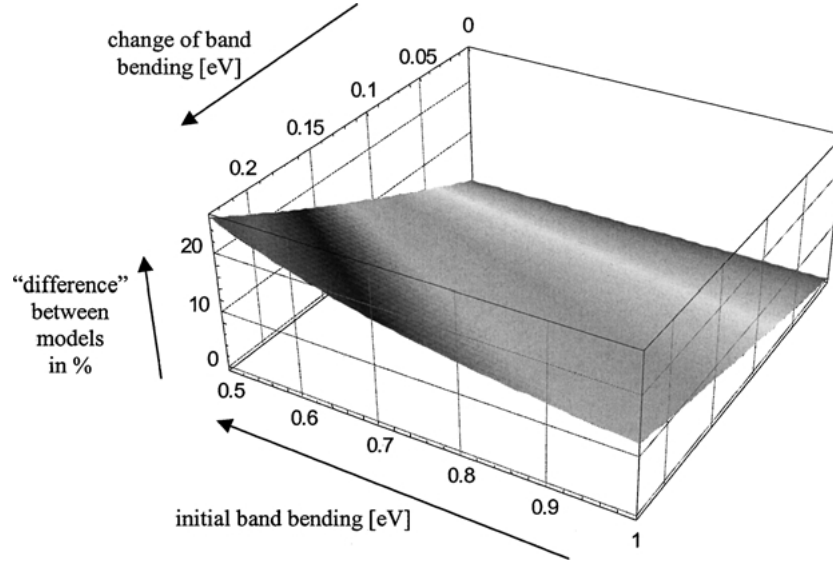
Fig. 12. Calculation of the "difference" (see Eq. (64)) between the Thermoelectronic Emission Theory and Diffusion Theory explained as a function of the initial band bending $V_{S,0}$ and the change in the band bending ΔV_S. The boundary conditions for the calculation are given in the text.

G_{diff} it turns out that there is a simple relation linked to n_S.

$$G_{\text{diff}} \sim V_S^{0.5} \cdot \exp\left(-\frac{q \cdot V_S}{k_B \cdot T}\right)$$

$$\approx \eta \cdot \left(\exp\left(-\frac{q \cdot V_S}{k_B \cdot T}\right)\right)^{\gamma} \sim n_S^{\gamma} \quad (65)$$

where η and γ are values which can be fitted for given temperatures. In the temperature range between 200°C and 400°C (typical operation temperatures) the value for η is around 0.45 and γ varies from 1.2 (at 200°C) to 0.8 (at 400°C).

To summarize, the following holds:

● Thermoelectronic Emission Theory: $G_{\text{thermo}} \sim n_S$
● Diffusion Theory: $G_{\text{diff}} \sim n_S^{\gamma}$

In fact, the equation for the Diffusion Theory is the more general one which leads for $\gamma = 1$ to the particular case of the Thermoelectronic Emission Theory. In general, the Diffusion Theory model is more appropriate since the depletion layer dimension for the materials under investigation is considerable larger than the mean free path of the electrons.

Here one can pick up the discussion of page 14, classifying the conduction across the grains in three different cases:

● For *case a*) using results above one obtains the relation between the conductance and the partial pressure of CO:

$$G \sim p_{\text{CO}}^{\frac{\beta \cdot \gamma}{\alpha + \delta}} \quad (66)$$

where the value of γ is in the range of 0.8 to 1.2.
● For *case b*), in the mentioned assumption of either V_S or a $V_{S,\text{effective}}$, one also ends up with the Eq. (66).
● For *case c*) the results are similar to the one described by the thick compact layer in Eq. (49).

4.2.3. Small grains. For small grains and homogeneous concentration of electrons, one has to examine *two cases* according to the ratio between the mean free path of electrons, λ, and the dimensions of the grains, $2 \cdot r$, taken for simplicity spherical. This criteria is related to the formula proposed by Many et al. [14] for the description of the influence of surface scattering on the mobility μ (where μ_b is the bulk value), which adapted to the geometry examined here is:

$$\mu = \frac{\mu_b}{1 + W \cdot \lambda/2 \cdot r} \quad (67)$$

where W is the probability of inelastic surface scattering. In the case of very small grains, the ratio $\lambda/(2 \cdot r)$ is

not negligibly small (see Table 1) so the influence of the surface scattering has to be taken into consideration. W is related to the deviation of the surface from a simple projection of the bulk. For the case discussed here, this deviation represents the difference between the concentration of scattering centres for electrons when they strike the surface and the concentration of scattering centres with which they interact when they move in the bulk of the grain. This scattering centre concentration difference is given by the charged oxygen species chemisorbed at the surface of the grains. If one uses the relation between W and θ proposed in [2]:

$$W \cong \theta \tag{68}$$

Equation (68) can be modified in the following way:

$$\mu \cong \frac{\mu_b}{1 + \theta \cdot \lambda/2 \cdot r} \tag{69}$$

using Eq. (35) which holds for small grains one obtains

$$\mu \cong \frac{\mu_b}{1 + \left(1 - \frac{n_S}{n_b}\right) \cdot \lambda/2 \cdot r} \tag{70}$$

A detailed analysis is still to be performed for the general case. The two aforementioned cases will correspond to:

- negligible value of $\lambda/(2 \cdot r)$, in which the only influence of surface phenomena in conductance will be in the concentration of electrons taking part in conduction. In this case, the conductance is proportional to the surface concentration of electrons n_S. This is given in this case by Eq. (40). Accordingly, the conductance will be:

$$G \sim p_{CO}^{\frac{\beta}{\alpha+1}} \tag{71}$$

- non-negligible value of $\lambda/(2 \cdot r)$, in which the influence of surface phenomena in conductance will originate from both mobility and concentration of electrons. In this case the conductance is proportional to the surface concentration of electrons n_S multiplied with the respective mobility.

It was shown in [2] that it is possible to obtain from Eq. (70) by expanding it to a Taylor series:

$$\mu \cong \left(\frac{\mu_b}{1 + \lambda/2 \cdot r}\right) \cdot \left(1 + \frac{\lambda}{2 \cdot r + \lambda} \cdot \frac{n_S}{n_b}\right) \tag{72}$$

with n_S given by Eq. (40). At higher CO concentrations, the conductance will be given by:

$$G \sim \left(p_{CO}^{\frac{\beta}{\alpha+1}} + \text{const}'' \cdot p_{CO}^{\frac{2\cdot\beta}{\alpha+1}}\right) \tag{73}$$

Equation (73) indicates that the influence of a surface phenomena modulated mobility causes a more complex dependence of the conductance on the CO partial pressure. This influence will depend on the values of the respective constants (see Eq. (72)) describing both the geometrical and electrical properties of the material.

4.3. Summary

To summarize the results on the sensing layer modelling there are three factors that will determine the actual relationship between the conductance of the sensing layer and the concentration of the gas species:

- surface chemistry, which means the interaction of the reacting gas species at the surface of the metal oxide and the associated charge transfer. This relates to the specific adsorbed oxygen species and how the oxidation of CO/sensing will take place. From the modelling point of view, it is described by quasi-chemical equations (see e.g. Eqs. (1) and (30)).
- The appearance of a depletion layer at the surface of the semiconductor material due to the equilibrium between the trapping of electrons in the surface states (associated with the adsorbed species) and their release due to desorption and the reaction with CO. From the modelling point of view, it is described by the Poisson and electro-neutrality equations (see e.g. Eqs. (6), (7) and (15)).
  ➤ Out of the first two factors, one can calculate the dependence of the electron concentration n_S in the depletion layer near the surface of the semiconductor as a function of the CO concentration (see Table 2).
- The conduction in the sensitive layer that translates the sensing into the measurable electrical signal. This strongly depends on the morphology of the sensitive layer and is summarized in Table 3.

Example.   Figure 13 presents one of the cases listed in Table 3; showing how the same surface chemistry (O^{--} reacting with CO) is transduced in different electrical signals depending on the characteristic of the sensing layer.

Table 3. Summary table of different cases discussed in the previous section.

| Reactive oxygen species	Compact layer			Porous layer			
	Thin		Thick	Large grains			Small grains
				With necks		Without necks	
	$q\Delta V_S \leq k_B T$	$q\Delta V_S > k_B T$		Open necks	Close necks		
	Mobility not influenced by surface phenomena						
$O_\beta^{-\alpha}$	$G \sim p_{CO}^{\frac{\beta}{\alpha+1}}$	$G \sim p_{CO}^{\frac{\beta}{\alpha+\delta}}$	$G = \xi - \sqrt{\zeta - \psi \cdot \frac{\beta}{\alpha+\delta} \cdot \ln p_{CO}}$	$G = \xi - \sqrt{\zeta - \psi \cdot \frac{\beta}{\alpha+\delta} \cdot \ln p_{CO}}$	$G \sim p_{CO}^{\frac{\beta \cdot \gamma}{\alpha+\delta}}$	$G \sim p_{CO}^{\frac{\beta \cdot \gamma}{\alpha+\delta}}$	$G \sim p_{CO}^{\frac{\beta}{\alpha+1}}$
O_2^-	$G \sim p_{CO}$	$G \sim p_{CO}^{2\ldots1.66}$	See above	See above	$G \sim p_{CO}^{2.4\ldots1.33}$	$G \sim p_{CO}^{2.4\ldots1.33}$	$G \sim p_{CO}$
O^-	$G \sim p_{CO}^{0.5}$	$G \sim p_{CO}^{1\ldots0.83}$	See above	See above	$G \sim p_{CO}^{1.2\ldots0.66}$	$G \sim p_{CO}^{1.2\ldots0.66}$	$G \sim p_{CO}^{0.5}$
O^{--}	$G \sim p_{CO}^{0.33}$	$G \sim p_{CO}^{0.5\ldots0.45}$	See above	See above	$G \sim p_{CO}^{0.6\ldots0.36}$	$G \sim p_{CO}^{0.6\ldots0.36}$	$G \sim p_{CO}^{0.33}$
	Mobility influenced by surface phenomena						
$O_\beta^{-\alpha}$	$G \sim (p_{CO}^{\frac{\beta}{\alpha+1}} + \tau \cdot p_{CO}^{\frac{2\beta}{\alpha+1}})$	No influence	No influence	No influence	No influence	No influence	$G \sim (p_{CO}^{\frac{\beta}{\alpha+1}} + \tau \cdot p_{CO}^{\frac{2\beta}{\alpha+1}})$
O_2^-	$G \sim (p_{CO} + \tau \cdot p_{CO}^2)$	No influence	No influence	No influence	No influence	No influence	$G \sim (p_{CO} + \tau \cdot p_{CO}^2)$
O^-	$G \sim (p_{CO}^{0.5} + \tau \cdot p_{CO})$	No influence	No influence	No influence	No influence	No influence	$G \sim (p_{CO}^{0.5} + \tau \cdot p_{CO})$
O^{--}	$G \sim (p_{CO}^{0.33} + \tau \cdot p_{CO}^{0.66})$	No influence	No influence	No influence	No influence	No influence	$G \sim (p_{CO}^{0.33} + \tau \cdot p_{CO}^{0.66})$
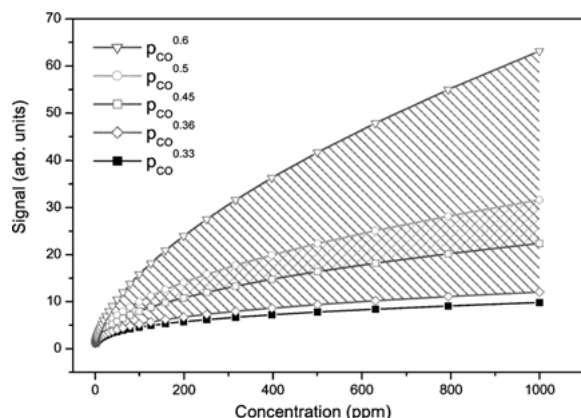
Fig. 13. Summarized calculated power law dependency for the different cases shown in Table 3 for the case of CO interaction with doubly ionized oxygen (O^{--}).

The solid black squares describe a situation corresponding to either (i) compact thin films or (ii) completely depleted small grains where, in both cases, the difference in band bending is lower that the thermal energy (flat band case). The crosshatched area indicates the range of exponents in the power law between 0.45–0.5, which is valid for thin, compact layers (completely depleted but not in flat band condition). The largest variation (simple hatched area) of the exponent between 0.36–0.6 corresponds to porous layers with large grains (interconnected by close necks or in point contacts).

The dependence of the conductance described up to now, holds for the homogenous sensitive layer without influence of contacts. The next section will also discuss this aspect in order to arrive at a complete modelling of the sensor.

5. Role of Contacts

As shown in Fig. 6 there is a resistance associated with the interface between the semiconducting sensitive layer and the metallic electrode. The importance of this resistance to the overall sensor resistance value depends on the morphological conditions. In what follows, the possible dependence of the contact resistance on the ambient atmosphere conditions is discussed in two sections:

The first is dealing only with the electrical contribution of the semiconducting sensitive layer–electrode interface to the overall sensor resistance.

The second describes the possible chemical influence of e.g. the catalytic activity of the contact material in the region close to the contacts.

5.1. Electrical Contribution

In this section, the objective is to determine whether there are changes in the contact resistance due to gas exposure. The assumptions are the following:
- The sensitive layer between the contacts is homogenous and the surface reactions are taking place in the same way all over
- Applying a measurement potential is not changing the situation described above

In the following, different cases of contacts between the electrode and the semiconducting sensing layer are discussed. The discussion is held rather general not being restricted to the particular case of SnO$_2$. For simplicity reasons (without limiting the validity), one has assumed a homogenous material allowing for the existence of both a depleted layer and of an unaffected bulk region. The work function of the semiconductor ϕ_S is defined by $\phi_S = (E_C - E_F)_b + qV_S + \chi$ where $(E_C - E_F)_b$ as bulk value is constant for all the cases as stated before. The work function of the metal ϕ_E is all cases considered to be higher than the work function value of the semiconducting sensitive layer ϕ_S (as assumed on the basis of experimental evidence).

When the metal electrode and the semiconducting sensitive layer are brought in contact, the electrons from the n-type semiconductor are flowing to the metal electrode resulting in an (additional) depletion layer at the interface in the semiconductor (reduced carrier concentration). The equilibrium of free charge carriers (electrons) is established levelling out the Fermi-energies to the equilibrium one (of course without an applied potential). From the energy band model point of view, this situation is described by the building of an (additional) band bending in the semiconductor ($q \Delta V_S$). Its value is equal to the initial difference of the Fermi-energies (measured from the vacuum level E_{Vac}).

In the following three different cases of bringing a metal electrode in contact with a semiconducting sensitive layer will be described.

Case 1, shown in Fig. 14, is giving the situation before and after the contact between the metal electrode and the semiconducting sensitive layer, which is initially in flat band condition.
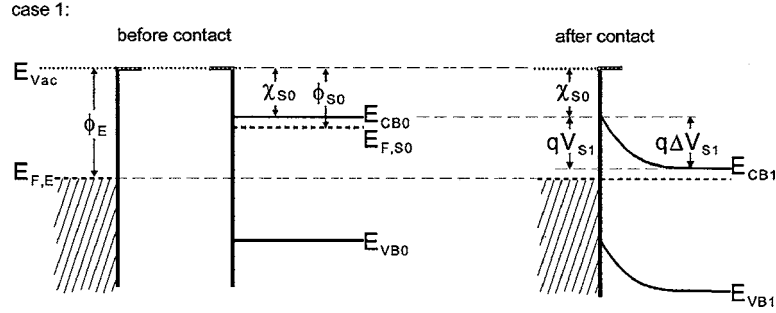
case 1:

Fig. 14. Situation before (left) and after contact (right) between the metal electrode and the semiconductor in Case 1 (for a flat band semiconductor). The work function ϕ of the semiconductor is changed after contact and gets to the value of the metal at the interface.

The electron affinity of the semiconductor at the interface χ_{S0} remains constant before and after the contact and due to the levelling of the Fermi-Energy one gets the band bending $qV_{S1} = q\,\Delta V_{S1}$. Out of the right picture in Fig. 14 it can be seen easily

$$\phi_E = \chi_{S0} + q \cdot V_{S1} + (E_{CB1} - E_{F,E}) \qquad (74)$$

since no bulk changes were assumed it holds

$$(E_{CB1} - E_{F,E}) = (E_{CB0} - E_{F,S0}) \qquad (75)$$

and consequently one can write

$$q \cdot V_{S1} = q \cdot \Delta V_{S1} = \phi_E - (\chi_{S0} + (E_{CB0} - E_{F,S0}))$$
$$= \phi_E - \phi_{S0} \qquad (76)$$

The resistance associated with the metal-semiconductor contact R_C is directly linked to the band bending qV_{S1}:

$$R_{C1} \sim \exp\left(\frac{q \cdot V_{S1}}{k_B T}\right) = \exp\left(\frac{\phi_E - \phi_{S0}}{k_B T}\right) \qquad (77)$$

Case 2 is presented in Fig. 15 and the difference (as compared to the first case) is an initial band bending at the semiconductor surface qV_{S2}. After the establishment of the contact the equilibrium is reached by a further band bending $q\Delta V_{S3}$. The final band bending is qV_{S3}, which can be calculated according to the following formula,

$$q \cdot V_{S3} = q \cdot V_{S2} + q \cdot \Delta V_{S3} = q \cdot V_{S2} + \phi_E - \phi_{S2} \qquad (78)$$

when making use of the same type of relation as given in Eq. (75). One can express ϕ_{S2} as

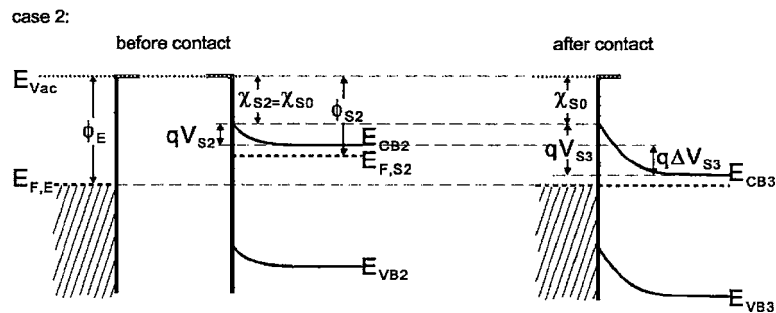$$\phi_{S2} = \phi_{S0} + q \cdot V_{S2} \qquad (79)$$

case 2:

Fig. 15. Situation before (left) and after contact (right) between the metal electrode and the semiconductor. Case 2 for a semiconductor, which show already a band bending before contact. Here no changes in the electronic affinity χ are assumed. The work function ϕ of the semiconductor is changed after contact and gets to the value of the metal at the interface.

Combining Eqs. (78) and (79) one obtains

$$q \cdot V_{S3} = q \cdot V_{S2} + \phi_E - \phi_{S0} + q \cdot V_{S2}$$
$$= \phi_E - \phi_{S0} = q \cdot V_{S1} \qquad (80)$$

So one can deduce that for cases 1 and 2 the contact resistance values R_C are equal ($R_{C1} = R_{C3}$).

One can generalise that different initial band bending values will all result in the same potential barrier at the contact. The value is determined by the bulk values of the work functions (both of metal and semiconductor). Once the pinning of Fermi-levels (and hence the contact band bending) is established (by getting the materials in contact) subsequent changes of the surface band bending of the semiconducting sensitive layer will not change the conditions at the metal-semiconductor interface. Accordingly the contact resistance will not be changed by surface interactions affecting the surface band bending.

Case 3 is depicted in Fig. 16. This is different from cases 1 and 2 since in the initial state the electronic affinity χ_{S4} is different from χ_{S0} with $\pm\Delta\chi$. In case 3, χ_{S4} is smaller than χ_{S0}. The effect on the contact resistance will be calculated in what follows:

$$q \cdot V_{S5} = q \cdot \Delta V_{S5} = \phi_E - \phi_{S4} \qquad (81)$$

$$\chi_{S4} = \chi_{S0} - \Delta\chi \qquad (82)$$

ϕ_{S4} can be expressed by (taking also an inherent part of Eq. (76))

$$\phi_{S4} = \chi_{S4} + (E_{CB4} - E_{F,S4})$$
$$= \chi_{S0} - \Delta\chi + (E_{CB0} - E_{F,S0})$$
$$= \phi_{S0} - \Delta\chi \qquad (83)$$

Combining Eqs. (81) and (83) and comparing with Eq. (76) one gets:

$$q \cdot V_{S5} = \phi_E - \phi_{S0} + \Delta\chi = q \cdot V_{S1} + \Delta\chi \qquad (84)$$

Equation (84) shows the increase of the final contact band bending by the value $\Delta\chi$ as compared to cases 1 and 2. Consequently the contact resistance R_{C1} is increased to R_{C5} according to:

$$R_{C5} \sim \exp\left(\frac{q \cdot V_{S1} + \Delta\chi}{k_B T}\right)$$

Following this consideration it can be stated that initial differences in the electronic affinity values are influencing the contact resistance. Once the contact is established, subsequent changes of the electronic affinity of the semiconducting sensitive layer (e.g. by adsorption of surface dipoles) may or may not influence the conditions at the metal-semiconductor interface. This depends on the relation between the action radius of the dipoles, their proximity to the metal-semiconductor interface and the given morphology/geometry at the contact.

The starting point for some straightforward calculations is the principle of superposition for potentials as given by

$$V = \sum_{i=1}^{N} V_i = \frac{1}{4\pi\varepsilon_0} \sum_i \frac{q_i}{r_i} \qquad (85)$$

For an elementary charge, one obtains the well-known Coulomb potential

$$V = \frac{1}{4\pi\varepsilon_0} \frac{q}{r} \qquad (86)$$
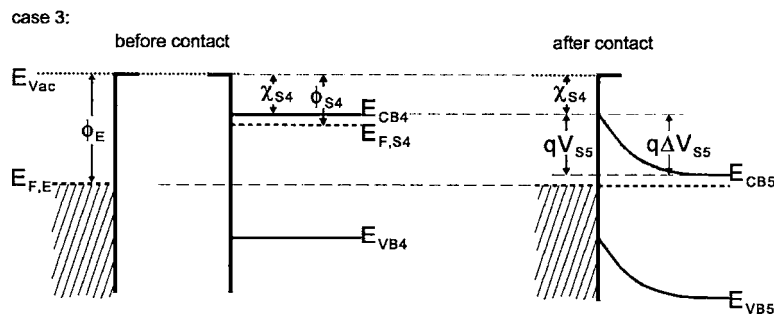

Fig. 16. Situation before (left) and after contact (right) between the metal electrode and the semiconductor. Case 3 for a flat band semiconductor with a different electron affinity χ_{S4} as compared to case 1. The work function ϕ is changed after contact and gets to the value of the metal at the interface.
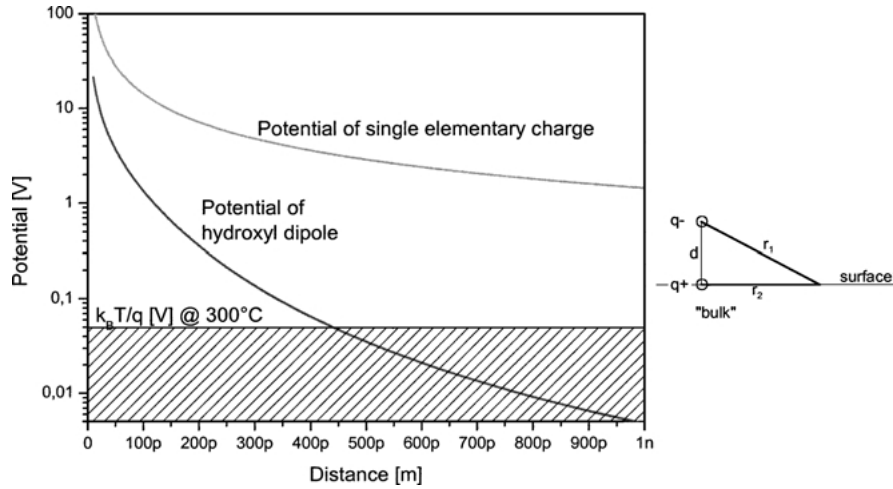
Fig. 17. Calculation of potential curves for a single elementary charge (at the position q^+ in the little figure on the right) for a hydroxyl dipole (q^+, q^-, as in the orientation in the little figure on the right). The hatched area is giving the potential of the thermal energy. The charge q^+ is giving the origin of the abscissa; the distance values plotted are given by r_2. Further explanation of calculations and results are given in the text.

where $r = r_2$ and q is in the position of q^+ in Fig. 17. Calculating the potential of a dipole based upon Eq. (85) one obtains the following relation:

$$V = \frac{1}{4\pi\varepsilon_0}\left(\frac{q}{r_2} + \frac{-q}{r_1}\right) = \frac{q}{4\pi\varepsilon_0}\frac{r_1 - r_2}{r_1 r_2} \qquad (87)$$

Since only surface positions are considered, r_1 can be expressed by

$$r_1 = \sqrt{d^2 + r_2^2} \qquad (88)$$

combining Eqs. (87) and (88), one obtains

$$V = \frac{q}{4\pi\varepsilon_0}\frac{\sqrt{d^2 + r_2^2} - r_2}{r_2\sqrt{d^2 + r_2^2}} \qquad (89)$$

with the dependency on r_2.

The values of q for the Coulomb potential and the dipole potential are different. As a standard, the Coulomb potential was calculated with a single elementary charge at the origin in the position of q^+ (1.6×10^{-19}C). For a surface dipole ($Sn^+ - OH^-$), the value of the dipolar moment μ is taken from literature [15] as 5.478×10^{-20}Cm ($=1.66$ Debye). Assuming a typical distance d of 200 pm (see e.g. [16]) one ends up with effective charges q^+ and q^- of the dipole at 2.739×10^{-20}C (about 17% of elementary charge).

Using these figures, the potential curves in Fig. 17 were calculated.

As expected, the range of interaction is substantially larger for the Coulomb potential as for the described surface dipole. If compared with the potential caused by the thermal energy at 300°C, the range of interaction is below 450 pm. So, only in absolutely close vicinity of the contact point between metal and semiconductor, there is a very small range of interaction possible. If typical values of the lateral contact area between grains and the metal electrode material are assumed to be at least several nanometers, the "influence potential" due to surface dipole is very limited. For "normal" contact areas expected to be in the order of nanometers (even for the material with the smallest grain size) the influence of surface dipole interaction with contacts will be in the noise of the measurement. Exceptions to this situation are extremely thin films (e.g. might be caused by shadowing effects during deposition near the electrode) where the thickness of the sensitive film close to the electrodes is in the range of the action radius of the dipoles (film thickness 1 nm and below).

To summarize, one can state that the changes of the electrical resistance attributed to the contacts are negligible during the operation of the sensor. The value of the contact resistance is established during the preparation. This value, in contrast to its change, might be important in the overall resistance of the sensor and could even decrease the sensor response by being a

"dead" series element, especially for the case of compact films where $z_g > z_0$. The whole discussion holds of course only if the boundary conditions stated at the beginning of this section are fulfilled.

A clear violation of the boundary condition could appear due to the chemical sensitisation/catalytic effect of the electrodes. This case will be discussed in the following section.

5.2.   *Chemical Contribution*

The reasons for chemical effects at the electrode sensing layer interface are related to the catalytic nature of the electrode material. The materials used are often platinum and gold. Several effects could be taken into consideration:

- Surface species, which can be more easily adsorbed on the electrode metal, may diffuse fast to the three-phase boundary where it can react with the partner adsorbed on the metal oxide sensitive layer. Thus the increased diffusion will lead to a higher catalytic conversion rate, which will be monitored by the electrical readout.
- Another effect is the increased production ("Catalysis") of reaction partners by the metal electrode material (for Pt but not for Au). This can happen by e.g. breaking of hydrocarbons in more active radicals. Hence the reaction partners can diffuse to the three phase boundary (electrode/sensing layer/gas phase) and consequently this region becomes "more active" in gas detection.
- In contrast to the above mentioned effects that will enhance the sensor response, it is possible that an increased catalytic reaction on the electrode material with a direct desorption from there, will lead to a gas consumption which is not monitored by the electrical readout. In consequence, this gas consumption may lead to an overall lowering of the analyte (depending on the given setup) and may thus even lead to a lowering of the sensor signal.

6.   Conclusion

The overall conduction in a sensor element is determined by the surface reactions, the resulting charge transfer processes with the underlying semiconducting material, and the transport mechanism within the sensing layer. The latter can be even influenced by the electrical and chemical electrode effects. The potential substrate effect, which means an interaction between the sensing layer and the underlying substrate material, was not considered. The reason for that is the lack of experimental evidence.

To summarize the full content of this paper, the different contributions are briefly recapitulated:

- The base of the gas detection is the interaction of the gaseous species at the surface of the semiconducting sensitive metal oxide layer. It is important to identify the reaction partners and the input for this is based upon spectroscopic information. Using this input, one can model the interaction using the quasi-chemical formalism. This is described in Section 3.
- As a consequence of this surface interaction, charge transfer takes place between the adsorbed species and the semiconducting sensitive material. This charge transfer can take place either with the conduction band or in a localized manner. In the first case, the concentration of the free charge carriers will be influenced. This was described in terms of n_S and e.g. summarized for oxygen in Table 2. For the understanding of the detection it is important also to deepen out insight in the localized charge transfer case. The latter case (in contrast to the first one) will have no direct impact on the conduction.
- In turn, the change of the concentration of the free charge carriers is translated into a change of the overall resistance of the sensing layer. The transfer function depends on the morphology of the layer. Section 4 is classifying the different cases and the results are summarized in Table 3.
- The overall resistance of the sensor will comprise the above-mentioned phenomena combined with the influence of the electrodes. Their influence depends on the morphology of the sensing layer, the geometrical arrangement, and the possible chemical effects. This was discussed in Section 5.

This modelling approach should guide experimental work, being conducted at various places worldwide.

References

1. G. Sberveglieri, *Sensors and Actuators B*, **6**, 239 (1992).
2. N. Bârsan, *Sensors and Actuators B*, **17**, 241 (1994).
3. M. Bauer, N. Bârsan, K. Ingrisch, A. Zeppenfeld, I. Denk, B. Schuman, U. Weimar, and W. Göpel, *Proc. of the 11th European Microelectronic Conference* (1997).
4. U. Hoefer, K. Steiner, and E. Wagner, *Sensors and Actuators B*, **26/27**, 59 (1995).
5. S.R. Morrison, *The Chemical Physics of Surfaces*, 2nd edn. (Plenum Press, New York, 1990).

6. G. Heiland and D. Kohl, in *Chemical Sensor Technology*, Vol. 1, edited by T. Seiyama (Kodansha, Tokyo), Ch. 2, pp. 15–38.

7. V.A. Henrich and P.A. Cox, *The Surface Science of Metal Oxides* (University Press, Cambridge, 1994), pp. 312–316.

8. M. Egashira, M. Nakashima, and S. Kawasumi, *J. Chem. Soc. Chem. Comm.* 1047 (1981).

9. N. Bârsan and R. Ionescu, *Sensors and Actuators B*, **12**, 71 (1993).

10. S. Lenaerts, M. Honore, G. Huyberechts, J. Roggen, and G. Maes, *Sensors and Actuators B*, **18/19**, 478 (1994).

11. A. Broniatowski, in *Polycrystalline Semi-Conductors*, edited by G. Harbeke (Springer Solid State Sciences Series, Vol. 57), (Hardcover - April 1985).

12. A. Broniatowski, in *Polycrystalline Semi-Conductors*, edited by G. Harbeke (Springer Solid State Sciences Series, Vol. 57), (Hardcover - April 1985).

13. R. Stratton, *Proc. Phys. Soc. B*, **69**, 513 (1956).

14. A. Many, Y. Goldstein, and N.B. Grover, *Semiconductor Surfaces* (Interscience, New York, 1965), p. 308.

15. H. Geistlinger, I. Eisele, B. Flietner, and R. Winter, *Sensors and Actuators B*, **34**, 499–505 (1996).

16. A.F. Hollemann and E. Wieberg, *Lehrbuch der Anorganischen Chemie*, 101th edn. (Walter de Gruyter, Berlin, 1995), p. 1592.

17. M. Schweizer-Berberich, PhD Thesis, Universität Tübingen, 1998.

18. W. Göpel and K.D. Schierbaum, *Sensors and Actuators B*, **26/27**, 1 (1995).

19. S. Lenaerts, J. Roggen, and G. Maes, *Spectrochimica Acta Part A-Molecular Spectroscopy*, **51**, 883 (1995).

20. J.P. Joly, L. Gonszalez-Cruz, and Y. Arnaud, *Bulletin de la Société Chimique de France*, 11 (1986).

21. B. Gillot, C. Fey, and D. Delafosse, *Journal of Chemical Physics*, **73**, 19 (1976).

22. N. Yamazoe, J. Fuchigami, M. Kishikawa, and T. Seiyama, *Surf. Sci.*, **86**, 335 (1979).

23. A.M. Volodin and A.E. Cherkasin, *Reac. Kinet. Catal. Lett.*, **17**, 329 (1981).

24. S.C. Chang, *J. Vac. Sci. Technol.*, **17**, 366 (1980).

25. D. Kohl, in *Gas Sensors* edited by, G. Sberveglieri (Kluwer, Dordrecht, 1992) ch. 2, p. 43.

26. M. Egashira, M. Nakashima, and S. Kawasumi, *J. Chem. Soc. Chem. Comm.*, 1047 (1981).

27. K. Morishige, S. Kittaka, and T. Morimoto, *Bull. Chem. Soc. Japan*, **53**, 2128 (1980).

28. A. Guest, PhD Thesis University of Nottingham, 1985.

29. E.W. Thornton and P.G. Harrison, *J. Chem. Soc. Faraday Trans.*, **71**, 461 (1975).

30. F. Berger, E. Beche, R. Berjoan, D. Klein, and A. Chambaudet, *Applied Surf. Sci.*, **93**, 9 (1996).

31. J.F. Boyle and K.A. Jones, *Electron. Mater.* **6**, 717 (1977).

32. S.J. Gentry and T.A. Jones, *Sensors and Actuators*, **10**, 141 (1986).

33. H. Windischmann and P. Mark, *J. Electrochem. Soc.: Solid-State Sci. Technol.*, **126**, 672 (1979).

34. M.J. Willett, in *Techniques and Mechanisms in Gas Sensing*, Vol. 3, edited by D.E. Williams and P.T. Moseley, J.O.W. Norris (Adam Hilger, Bristol, 1991), p. 61.